AD-A049 506 NAVAL RESEARCH LAB WASHINGTON D C F/G 9/1
CALCULATION OF OPTIMUM OPERATING PARAMETERS FOR A GYROTRON TRAV--ETC(U)
OCT 77 K R CHU, A T DROBOT, V L GRANATSTEIN

UNCLASSIFIED NRL-MR-3553 SBIE-AD-E000 092 NL

1 OF 1
ADA049506

END
DATE FILMED
3-78
DDC

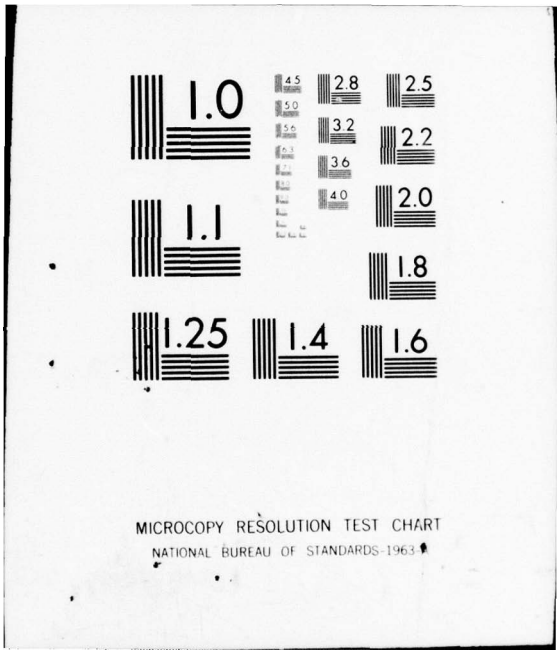
1.0
4.5
5.0
5.6
2.8
3.2
3.6
4.0
2.5
2.2
2.0
1.8
1.1
1.25
1.4
1.6
MICROCOPY RESOLUTION TEST CHART
NATIONAL BUREAU OF STANDARDS-1963

NRL Memorandum Report 3553

Calculation of Optimum Operating Parameters for a Gyrotron Travelling Wave Amplifier

K. R. Chu and A. T. Drobot

Science Applications, Incorporated
McLean, Virginia 22101

and

V. L. Granatstein and J. L. Seftor

Plasma Physics Division

October 1977

NAVAL RESEARCH LABORATORY
Washington, D.C.

SECURITY CLASSIFICATION OF THIS PAGE (When Data Entered)

REPORT DOCUMENTATION PAGE

READ INSTRUCTIONS BEFORE COMPLETING FORM

1. REPORT NUMBER: NRL Memorandum Report 3553
2. GOVT ACCESSION NO.
3. RECIPIENT'S CATALOG NUMBER
4. TITLE (and Subtitle): CALCULATION OF OPTIMUM OPERATING PARAMETERS FOR A GYROTRON TRAVELLING WAVE AMPLIFIER
5. TYPE OF REPORT & PERIOD COVERED: Interim report on a continuing NRL problem
6. PERFORMING ORG. REPORT NUMBER
7. AUTHOR(s): K.R. Chu,* A.T. Drobot,* V.L. Granatstein and J.L. Seftor
8. CONTRACT OR GRANT NUMBER(s): NRL-MR-3553
9. PERFORMING ORGANIZATION NAME AND ADDRESS: Naval Research Laboratory, Washington, D.C. 20375
10. PROGRAM ELEMENT, PROJECT, TASK AREA & WORK UNIT NUMBERS: NRL Problem R08-92; Project No. XF54-587 091; PE62762N
11. CONTROLLING OFFICE NAME AND ADDRESS: Naval Electronic Systems Command, Washington, D.C. 20360
12. REPORT DATE: Oct[illegible]77
13. NUMBER OF PAGES: 27
14. MONITORING AGENCY NAME & ADDRESS (if different from Controlling Office): XF54581, F82302
15. SECURITY CLASS. (of this report): UNCLASSIFIED
15a. DECLASSIFICATION/DOWNGRADING SCHEDULE
16. DISTRIBUTION STATEMENT (of this Report): Approved for public release; distribution unlimited. XF54581091, SF32302418
17. DISTRIBUTION STATEMENT (of the abstract entered in Block 20, if different from Report)
18. SBIE
19. AD-E000 092

DDC RECEIVED FEB 6 1978 B

18. SUPPLEMENTARY NOTES: *Science Applications Incorporated, McLean, Virginia 22101

19. KEY WORDS (Continue on reverse side if necessary and identify by block number)
Cyclotron Maser
Gyrotron
Millimeter Wave Generation
TE(01)

20. ABSTRACT (Continue on reverse side if necessary and identify by block number)

Optimum operating parameters are determined for a new type of high power, high efficiency generator of millimeter waves known as a gyrotron travelling wave amplifier. In the example considered, wave amplification results from the interaction of a TE_{01} waveguide mode with the fundamental cyclotron harmonic of an electron beam. The parameter optimization involves the determination of the point of maximum device efficiency as a function of beam density, beam energy, beam positioning, and external magnetic field for the output power required. An analytical linear theory and a numerical simulation code form the basis of theoretical calculations. As a result of the
(Continued)

DD FORM 1 JAN 73 1473 EDITION OF 1 NOV 65 IS OBSOLETE
S/N 0102-LF-014-6601

SECURITY CLASSIFICATION OF THIS PAGE (When Data Entered)

251 950

20. Abstract (Continued)

extensive survey in parameter space, the peak efficiency in the beam frame has been found to exceed 70%. This result has been applied to the specific design of a 35 GHz amplifier with output power ~340 kW, a power gain of 2 db/cm, and a laboratory frame efficiency of 51%.

CONTENTS

CALCULATIONS OF OPTIMUM OPERATING PARAMETERS FOR A GYROTRON TRAVELLING WAVE AMPLIFIER*

I. INTRODUCTION

The gyrotron is a new type of microwave device employing the electron cyclotron maser mechanism. It ideally consists of an ensemble of monoenergetic electrons following helical trajectories around the lines of an axial magnetic field inside a fast wave structure such as a metallic tube or waveguide. The physical mechanism responsible for the radiation in the gyrotrons has its origin in a *relativistic* effect. Initially, the phases of the electrons in their cyclotron orbits are random, but phase bunching can occur because of the dependence of electron cyclotron frequency on the relativistic electron mass. Those electrons that lose energy to the wave become lighter, rotate faster, and hence accumulate phase lead while those electrons that gain energy from the wave become heavier, rotate slower, and accumulate phase lag. This can result in phase bunching such that the electrons radiate coherently and amplify the wave. Energy transfer from the electrons to the wave is optimized when $\omega - k_z v_z - s\Omega_b \geq 0$, where $\omega, k_z, v_z, s, \Omega_b$ are respectively, the wave frequency, axial wave number, axial electron velocity, cyclotron harmonic number and relativistic electron cyclotron frequency. Early descriptions of the physical process are to be found in the works of Twiss[1], Schneider[2], and Gapanov[3], while the first deliberate experimental study was made in 1964 by Hirshfield and Wachtel[4]. An extensive description of the early work is to be found in recent review papers[5,6].

*Work supported in part by the Naval Electronic Systems Command, Task XF 54-587, by the Army Ballistic Missile Defense Advanced Technology Center, MIPR W31RPD-73-Z787, and by the Naval Surface Weapons Center (Dahlgren), Task SF32-302-41B.

Manuscript submitted June 29, 1977.

The gyrotron emits radiation near the frequency $\omega = \Omega_b + k_z v_z$, so the wavelength is primarily determined by the strength of the applied magnetic field and not by the dimensions of a resonant structure. Thus unlike most other microwave tubes, the internal dimensions of the device may possibly be large compared to the wavelength, and high power handling capability becomes compatible with operation at millimeter and submillimeter wavelengths. Indeed, the highest recorded millimeter wave power, both peak and average, have been attained in gyrotron devices. The high peak powers were achieved in a series of experiments using intense relativistic electron beams ($V \sim 1$ MV, $I \sim 30$ kA) and powers achieved include 900 MW at $\lambda = 4$ cm[7], 350 MW at $\lambda = 2$cm[8], 8 MW at $\lambda = 8$mm[9], and 2 MW at $\lambda = 4$ mm[9]; however, efficiency of converting electron beam energy to EM radiation was only $\sim$ 1%. On the other hand, the high average powers were generated with high efficiency and with current and voltage levels similar to those in conventional microwave tubes; thus, the high average power work leads directly to practical devices.

The initiative in developing high average power gyrotron was first taken by workers at the Gorkii State University (USSR)[10,11]. The key to achieving efficient devices was careful design of the electron gun. In the Gorkii studies, a crossed field "magnetron injection gun" was used to launch an annular electron beam with large fraction of energy transverse to the axis and with minimum energy spread. Work on nonuniform cross-section open resonators to optimize beam-wave coupling has also taken place[11]. All together these developments have led to demonstration of a technological breakthrough in CW millimeter wave generation. Using a superconducting magnet, Zaytsev, et. *al.*[10] have generated the following CW powers: 12 kW at $\lambda = 2.78$ mm with 31% efficiency; 2.4 kW at $\lambda = 1.91$ mm with 9.5% efficiency; and 1.5 kW at $\lambda = 0.92$ mm with 6.2% efficiency. Other impressive results by Soviet workers include the operation of a second harmonic device in a magnetic field of only 6 kG which produced at $\lambda =$ 9 mm a CW power of 10 kW with 40% efficiency[11]. Figure 1 compares these results with CW

power available from other microwave devices; an advance in CW power capability by 3 to 5 orders of magnitude is clearly indicated.

The Soviet gyrotrons have operated as oscillators using a single resonant cavity as the r.f. structure. However, the gyrotron process lends itself to the use of a variety of r.f. structures[6], and can operate as an amplifier as well as an oscillator. In Fig. 2 schematics of three types of gyrotrons are sketched. The gyromonotron in Fig. 2a corresponds to the Soviet oscillator configuration. Figure 2b shows the 2-cavity gyroklystron amplifier which induces a transverse phase bunching in an input cavity, allows the bunching to continue ballistically between cavities and then converts transverse electron energy to wave energy in an output cavity. Operation of such a device was reported in an early experiment by Wachtrel and Hirshfield[12], and recently by Jory[13].

A third type of gyrotron, on which this paper focuses, is the gyrotron travelling wave amplifier (gyro-TWA, Fig. 2c). This device is especially uncomplicated in that the r.f. structure is a simple waveguide. It has a clear advantage in handling high power since the field strengths encountered for a given power level will be much lower in a travelling wave device than in a device employing resonant cavaties. Also, superior bandwidth and tunability characteristics are expected. The operation of a gyro-travelling wave amplifier was demonstrated in an experiment using an intense relativistic electron beam[14]. A gain of 16 dB (1.1 dB/cm) was achieved at 8.6 GHz with a bandwidth of $\sim$ 5% and an output power of 4 MW; there was also indication of octave-like tunability through changing the magnetic field in step with the input frequency. However, efficiency in this first gyro-TWA was low in part because of poor beam quality.

The present paper describes the design of a millimeter-wave gyro-TWA which is intended to be highly efficient. It is proposed to couple the r.f. structure designed here with a "mag-

netron injection gun" of the type used in the Gorkii studies so than an electron beam can be provided with sufficiently high quality to satisfy the design assumptions.

II. DESIGN CRITERIA AND THEORETICAL APPROACHES

The methods presented here for parameter optimization are generally applicable to gyrotron travelling wave amplifiers. As an illustration we will consider a particular example, namely, a gyrotron travelling wave amplifier aimed at the laboratory production of 340 kW (CW or pulsed) power at a frequency of 35 GHz. Wave amplification results from the interaction between the TE_{01} circular waveguide mode,

$$\omega^2 - k_z^2 c^2 - \omega_c^2 = 0, \tag{1}$$

and the fundamental cyclotron harmonic of the beam,

$$\omega - k_z v_z - \Omega_b = 0. \tag{2}$$

where ω_c is the cutoff frequency of the TE_{01} mode, $\Omega_b \equiv \Omega_e/\gamma$, $\Omega_e \equiv eB/mc$, and $\gamma \equiv [1 - (v_\perp^2 + v_z^2)/c^2]^{-1/2}$.

The principal design criterion is to attain high efficiency. To achieve this, it is desirable to select the magnetic field such that the two curves represented by Eqs. (1) and (2) intersect at a grazing or near grazing angle in the (ω, k_z) plane, i.e. with the group velocity $(k_z c^2/\omega)$ of the waveguide mode nearly equal to the beam velocity (v_z). The reason for such a choice will become evident.

Figure 3 shows the configuration of the beam-waveguide system on which our calculations are based. It consists of an annular electron beam propagating with uniform velocity v_z in a circular cross section waveguide of radius r_w. the system is immersed in an external magnetic field, $B_0\ e_z$, oriented along the axis of the waveguide. We assume that all electrons have the same perpendicular velocity $v_\perp$. Under the influence of the external magnetic field, the

electrons gyrate at the frequency Ω_b with the Larmor radius $r_L \equiv v_\perp/\Omega_b$. We assume that the guiding centers of all electrons are uniformly distributed on a surface of constant radius r_0. Thus the beam inner radius (r_1) and outer radius (r_2) are $r_1 = r_0 - r_L$ and $r_2 = r_0 + r_L$.

In this model, we have assumed a thin (thickness $= 2\ r_L$) monoenergetic electron beam. Our recent computer simulation of a carefully designed electron gun shows that a beam with thickness $\leqslant 2.3\ r_L$ and energy spread $<<$ 1% can be achieved (see Sec. V).

Calculations of the optimum operating parameters have been based on two independent approaches. First, a linear analytical treatment of the beam-wave interaction has been used to calculate the linear wave frequency, growth rate, and the beam position and wave number for maximum beam-wave coupling. As in earlier analyses[15-17], the presence of the beam is treated as a perturbation to the waveguide. However, the problem has now been formulated in realistic cylindrical geometry rather than the idealized parallel plate geometry previously adopted. This improvement in modelling is of considerable importance, since efficiency is a sensitive function of quantities which depend on geometrical factors. A second improvement in modelling is that we treat the electron guiding center radius r_0 as a variable parameter, while in earlier parallel-plate models[14-16], the guiding centers were centrally located between the plates. This gives us the means to optimize the beam-wave coupling with respect to r_0.

For generality, all the calculations have been done in the beam frame (i.e. the reference frame in which the beam axial velocity is zero). Furthermore, the following nomalization procedures are introduced, through which the waveguide radius r_w is scaled out of the problem:

$$\text{length normalized to } r_w \tag{3}$$

$$\text{frequency normalized to } c/r_w \tag{4}$$

$$\text{velocity normalized to } c \tag{5}$$

EM field normalized to mc^2/er_w.

(6)

The results obtained are thus applicable to any waveguide radius r_w and for any beam axial velocity v_z by the appropriate beam to lab frame transformation. In Appendix A we have included the transformation formulae for conversion from beam frame to lab frame quantities and from dimensionless to physical units.

To maintain a clear distinction between lab frame, beam frame, normalized and physical quantities the following notation has been adopted:

(i) Beam frame quantities are denoted by primed symbols (e.g., γ'), laboratory frame quantities are unprimed (e.g. γ).

(ii) Normalized dimensionless quantities are denoted by a bar (e.g. $\overline{\Omega}_b$). Unbarred symbols represent either physical quantities (e.g. Ω_b) or naturally dimensionless ones (e.g. γ).

The derivation of the linear dispersion relation is lengthy but straightward. Since the methods are analogous to those described in detail by Ott and Manheimer,[15] only the result will be presented here.

The normalized dispersion relation for the excitation of the TE_{01} mode at the fundamental electron cyclotron harmonic (expressed in beam frame) is

$$\bar{\omega}'^2 - \bar{k}_z'^2 - \bar{\omega}_c^2 = \frac{4\nu'}{\gamma' J_0^2(x_1)} \left[- \frac{(\bar{\omega}'^2 - \bar{k}_z'^2)\beta_\perp'^2 H(x_1\bar{r}_0, x_1\bar{r}_L)}{(\bar{\omega}' - \bar{\Omega}_b')^2} + \frac{\bar{\omega}' Q(x_1\bar{r}_0, x_1\bar{r}_L)}{\bar{\omega}' - \bar{\Omega}_b'} \right], \tag{7}$$

where $x_1 = 3.832$ is the first nonzero root of $J_1(x) = 0, \nu' \equiv N' r_e$ is a dimensionless beam density parameter (N' is the total number of electrons per unit length $r_e \equiv e^2/mc^2$ is the classical

electron radius), $\beta_\perp' \equiv v_\perp'/c$, and

$$H(x,y) \equiv [J_1(x)J_1'(y)]^2 \tag{8}$$

$$Q(x,y) \equiv 2H(x,y) + yJ_1'(y)J_1''(y)\{J_1^2(x)(1+x^{-2}) + [J_1'(x)]^2\}$$
$$+ 2J_1(x)J_1'(x)J_1'(y)[yJ_1'(y) - J_1(y)]/xy \tag{9}$$

Note that the primes in Eqs (8) and (9) represent, respectively, the first and second derivatives of the Bessel function J_1 with respect to its argument. Elsewhere else in this paper, the primes indicate beam frame quantity.

In Eq. (7), $\bar{r}_0, \bar{r}_L$, and $\bar{\omega}_c$ are frame independent quantities. It can be easily shown that the normalized cutoff frequency of the TE_{01} mode, $\bar{\omega}_c$, is numerically equal to x_1.

This analytical work has been complemented by a single wave numerical simulation code. The Cartesian version of this code was initially developed by Sprangle and Manheimer.[16] It was later refined by Sprangle and Drobot[17] and employed to investigate the saturation mechanisms. A complete documentation of the Cartesian code appears in Ref. 17. Here we have converted the code into cylindrical geometry and use it to simulate the beam-wave interaction processes until the wave reaches saturation. A self consistent value of the efficiency can therefore be determined. The simulation shows two different but simultaneously present saturation mechanisms —depletion of free electron energy and electron trapping in phase space. For a detailed description of these mechanisms, see Ref. 17. The values quoted for the efficiency in Sec. III are those taken from the simulation data. Conservation of energy was monitored in the code and never deviated by more than 0.1%. As a cross check, the linear frequency and growth rate obtained from Eq. (7) have been compared to the linear stages of the simulation. The agreement between the two approaches was very good. (see Sec. III).

III. BEAM FRAME PARAMETER OPTIMIZATION

As seen from Eq. (7), solutions of the problem in the beam frame and in dimensionless units require the specification of five parameters: $\bar{r}_0, \bar{k}_z', \nu', \gamma'$, and $\overline{\Omega}_b'$. In the present design, we will choose $\bar{r}_0$ and $\bar{k}_z'$ so that the beam-wave coupling, represented by the linear growth rate $\bar{\omega}_i'$, is a maximum with respect to these two parameters. The parameter ν' will be determined from the required output power. With these three parameters specified, the energy conversion efficiency η', defined as the ratio of the final wave energy to the initial beam energy, can be calculated numerically varying the two remaining parameters γ' and $\overline{\Omega}_b'$. The point in the $(\gamma', \overline{\Omega}_b')$ parameter space where η' peaks will then be chosen for the design.

The first term on the RHS of Eq. (7), proportional to $\beta_\perp'^2$, is the driving term for the instability. Hence, to maximize the beam-wave coupling with respect to $\bar{r}_0$, we let $\bar{r}_0 = 0.48$ so that $H(x_1 \bar{r}_0, x_1 \bar{r}_L)$ peaks. This is also the radius at which the wave electric field $\bar{E}_\theta'$ $[\alpha J_1(x_1 \bar{r})]$ peaks. We mention in passing that for operation at higher cyclotron harmonics, the optimum beam position does not in general coincide with the peak of the wave electric field.

The second term on the RHS of Eq. (7) imposes a threshold energy on the beam, below which there will be no instability. For most gyrotron devices including the presently designed one, the beam is well above threshold energy. Hence this term can be neglected. We expand $\overline{\Omega}_b$ about a fixed value $\overline{\Omega}_{b0}$, and expand $\bar{\omega}'$ and $\bar{k}_z'$ about the intersecting point $(\bar{\omega}_0', \bar{k}_{z0}')$ of the two equations,

$$\bar{\omega}'^2 - \bar{k}_z'^2 - \bar{\omega}_c^2 = 0 \tag{10}$$

and

$$\bar{\omega}' - \overline{\Omega}_{b0}' = 0 \tag{11}$$

Substituting

$$\bar{\omega}' = \bar{\omega}_0' + \Delta\bar{\omega}'$$

$$\bar{k}_z' = \bar{k}_{z0}' + \Delta\bar{k}_z'$$

$$\bar{\Omega}_b' = \bar{\Omega}_{b0}' + \Delta\bar{\Omega}_b'$$

into Eq. (7) and keep terms to first order in $\Delta\bar{\omega}'$, $\Delta\bar{k}_z'$, and $\Delta\bar{\Omega}_b'$, we obtain

$$\left(\Delta\bar{\omega}' - \frac{\bar{k}_{z0}'}{\bar{\omega}_0'}\Delta\bar{k}_z'\right)(\Delta\bar{\omega}' - \Delta\bar{\Omega}_b') = \frac{-2\nu' x_1^2 H\beta_\perp'^2}{\gamma' J_0^2(x_1)\bar{\omega}_0'}, \tag{12}$$

In Eq. (12), $\Delta\bar{\omega}' = \Delta\bar{\omega}_r' + i\Delta\bar{\omega}_i'$ is a complex number, while all other quantities are real. Differentiating Eq. (12) with respect to $\Delta\bar{k}_z'$, we obtain

$$\frac{d(\Delta\bar{\omega}')}{d(\Delta\bar{k}_z')} = \frac{\bar{k}_{z0}'(\Delta\bar{\omega}' - \Delta\bar{\Omega}_b')}{\bar{\omega}_0'(3\Delta\bar{\omega}' - \Delta\bar{\Omega}_b' - 2\bar{k}_{z0}'\Delta\bar{k}_z/\bar{\omega}_0')}, \tag{13}$$

Eq. (13) shows that if $\bar{k}_{z0}' = 0$, the growth rate $\Delta\bar{\omega}_i'$ is a maximum regardless of the values of $\Delta\bar{k}_z'$ and $\Delta\bar{\Omega}_b'$, i.e., $\Delta\bar{\omega}_i'$ remains a maximum with respect to $\bar{k}_z'$ even with small variations in $\bar{\Omega}_b'$. In comparison, if $\bar{k}_{z0}' \neq 0$, $\Delta\bar{\omega}_i'$ peaks [i.e. the RHS of Eq. (13) is real] only when $\Delta\bar{k}_z' = \Delta\bar{\Omega}_b' = 0$. The case $\bar{k}_{z0}' = 0$ thus has the advantage of insuring maximum growth rate (with respect to $\bar{k}_z'$) when the magnetic field is varied to optimize the efficiency. It implies a grazing intersection of the two curves represented by Eqs. (10) and (11) (see Fig. 4). This explains why we have chosen a grazing or near grazing intersection for the design.

It is convenient to define a new parameter X':

$$X' \equiv \Omega_b'/\omega_c.$$

When the applied magnetic field is such that $X' = 1$ the two curves [Eq. (10) and (11)] intersect at an exact grazing angle.

We now consider the choice of ν'. For each value of ν', one can calculate the point in (γ', X') space where η' peaks. Given the beam axial velocity v_z in the lab frame, the beam power (P_b) and the output wave power (P_w) at the point of maximum efficiency can then be calculated [see Appendix A, Eqs. (A5-7)]. To specify v_z, we define a lab frame parameter α,

$$\alpha \equiv v_\perp / v_z .$$

Thus, for a fixed value of α, there is a one to one correspondence between P_w and ν'. Lengthy calculations are required to deduce ν' from P_w because one might have to scan a range of values for ν' before finding the one that yields the prescribed P_w. In practice, however, one can make a close initial guess for ν' on the basis of the required output wave power, the expected efficiency and beam energy [see Eqs. (A5-7)], and then proceed to calculate the optimum γ', X', and P_w. If P_w turns out to be too large, for example, by 10%, then the next guess for ν', 10% smaller, can be very accurate because the relation between P_w and ν' is almost linear. If there is an acceptable range of P_w, the initial guess of ν' usually suffices.

The choice for the velocity ratio α is guided by two considerations - having as much energy in the perpendicular gyromotion as possible and minimizing the beam temperature spread. The second consideration sets an upper limit on α. Our electron gun simulation code showed that for $\alpha > 1.5$, the beam temperature began to increase rapidly and was no longer suitable. Thus we let $\alpha = 1.5$. The required output wave power is $\sim$ 300 kW, which corresponds to $\nu' \simeq 0.002$, if we assume $\gamma' \simeq 1.1$ and a 45% efficiency. Thus we let $\nu' = 0.002$ be our initial guess. We now present the calculations that lead to the optimized γ', X', and P_w for the initially chosen ν'. The calculated optimum P_w (340 kW) turns out to be about 11% larger than expected, but falls in the acceptable range.

With ν' specified at $\nu' = 0.002$ the efficiency η' has been calculated in a two parameter space (γ', X'). The results are summarized in Figures 5 and 6. Fig. 5 shows two plots of η' vs

γ'. The solid curve represents the efficiency for grazing interaction ($X' = 1$). It predicts a maximum efficiency $\eta' \simeq 42\%$ at $\gamma' = 1.04$. The dashed curve shows the efficiency as a function of γ' but for an optimized value of X'. The peak efficiency is now $\eta' \simeq 73\%$ at $\gamma' = 1.10$ and $X' \simeq 0.957$. It is interesting to note that the optimization in X' shifts the point of maximum efficiency to higher γ' than found for grazing interaction. Decreasing X' from 1 has the effect of delaying phase trapping[14], which is one of the two mechanisms responsible for saturation. Since phase trapping is more dominant at higher γ' this qualitatively explains why the efficiency peak moves to higher γ' with magnetic mismatching. To determine quantatively the value of γ' where the efficiency peaks, a thorough search of the (γ' , X') parameter space was required.

It can be seen in Fig. 5 that at the value of γ' for which the maximum efficiency was found a small variation in X' from 1.0 to 0.96 caused a large change in the efficiency from 30% to 70%. To further illustrate the sensitivity of the efficiency as a function of X' a graph of η' vs X' is shown in Fig. 6 for $\gamma' = 1.10$, the value corresponding to peak efficiency. It can be seen in Fig. 6 that η' is a sensitive function of X'. It increases sharply as X' is decreased from unity and then falls precipitously if X' is reduced too much. This occurs because for too low a value of X', the system becomes linearly stable. We would like to stress that for an experiment to operate near the peak value of η', it is essential to control parameters such as magnetic field, beam voltage and driver frequency within an accuracy of $\leqslant 1\%$.

Fig. 7 shows the growth rate ($\bar{\omega}_i'$) and the difference between wave frequency ($\bar{\omega}_r'$) and electron cyclotron frequency ($\overline{\Omega}_b'$) as a function of X' for the same parameters as used in Fig. 6. Solid curves are calculated from Eq. (7) and the solid data points are taken from the simulation runs. The agreement between analytical and simulation results is found to be very good for the runs shown in this figure as well as for all other runs. From Figs. 6 and 7, we observe that when the efficiency approaches a maximum as a result of varying X', the growth rate approaches zero. Too low a growth rate is clearly undesirable. However, as one moves slightly

away from the peak efficiency, the growth rate increases rapidly. Some compromise must be made between growth rate and efficiency in selecting the operating point. For the designed amplifier, we have chosen the point $X' = 0.96$ where the efficiency is $\eta' = 70\%$, only three percent below the peak value. As will be shown, this point corresponds to a reasonably high power gain (2 dB/cm). The other parameters corresponding to this point are: $\nu' = 0.002$, $\bar{r}_o = 0.48$, $\gamma' = 1.1$, $\bar{k}_z' = 0$, $\bar{\omega}_r' = 3.791$, and $\bar{\omega}_i' = 0.0342$.

IV. CONVERSION OF BEAM FRAME OPTIMUM PARAMETERS INTO DESIGN PARAMETERS

To convert the beam frame optimum parameters into actual design parameters, two peices of information are required:

(i) the beam axial velocity (in lab frame), which can be calculated from the previously specified value of α.

(ii) the waveguide radius, which is determined from the desired wave frequency, $f = 35$ GHz. [see Appendix A, Eq. (A-4)].

Using the conversion formulae tabulated in Appendix A, we have converted the optimum parameters obtained in Sec. II into the design parameters for a 35 GHz, 340 kW gyro-TWA. They are shown in Table 1.

The experimental configuration which was based on these design parameters is shown in Fig. 8. The entire device is placed within the bore of a superconducting magnet. This allows precise shaping of the magnetic field over the entire electron beam. Such control is essential because of the great impact small changes in the magnetic field have on both the device efficiency and the operation of the electron gun. The magnetic field profile shows a carefully designed compression region required to obtain a beam with the proper velocity ratio α. After

being compressed, the beam enters a uniform magnetic field region where the cyclotron maser mechanism operates. An external driver generates a r.f. signal which is injected at two azimuthal positions at the left end of the drift tube so as to launch a TE_{01} wave. The use of an absorber ensures that the wave can propagate in only one direction so as to prevent oscillations. Amplification occurs in the uniform field region to the right of the r.f. injection point. Beyond this region the electron beam is collected at the wall as the magnetic field falls off. Stray electrons are deflected by a small magnet. The r.f. signal continues down the drift tube and exits at the window.

V. DISCUSSION AND CONCLUSION

At this time there exists no comprehensive theory detailing the effects of beam temperature on the efficiency of gyro-TWA's. It is possible, however, on the basis of nonlinear saturation mechanisms to derive the following qualitative condition for the validity of the cold beam approximation [17]:

$$\delta\gamma'/\gamma' << 2(\gamma - 1)\eta/\gamma, \tag{14}$$

where $\delta\gamma'$ is the energy spread in the beam frame and η is the laboratory efficiency calculated for a cold beam. A numerical simulation has been made of the NRL gun (see Fig. 8), which is similar in configuration to the electron gun used by Kisel [11] et al. The beam produced in the simulation is almost monoenergetic [typically, $\delta\gamma/(\gamma - 1) << 1\%$] so that the energy spread in the beam frame ($\delta\gamma'$) is caused mainly by a velocity pitch angle spread $\delta\theta$ ($\theta \equiv \tan\alpha$) of the beam electrons. For the beam parameters in Table I, we find that $\delta\theta \simeq 0.049$ and $\delta\gamma/(\gamma - 1) \simeq 0.002$. When the beam energy spread (in lab frame) is much smaller than pitch angle spread, Eq. (14) can be replaced by [17]

$$\delta\theta << \frac{2(\gamma - 1)\eta(1 - \beta_z^2)}{\gamma\beta_z\beta_\perp}, \tag{15}$$

where $\beta_z \equiv v_z/c$ and $\beta_\perp \equiv v_\perp/c$.

Substituting the beam parameters in Table I into Eq. (15) gives

$$\delta\theta << 2.1\,\eta\,.$$

This is well satisfied since $\delta\theta \simeq 0.05$ and the projected value for η is ~ 0.5. The cold beam approximation adopted in our theory is therefore realistic based on the simulation studies of the electron gun.

In conclusion, we have formulated the linear cyclotron maser theory and a numerical simulation code in cylindrical geometry and shown, through an example, how all the parameters of a gyrotron device are optimized to achieve high efficiencies. The choice of beam position γ_o and wave number k_z are based on the condition of maximum linear beam-wave coupling. The beam density parameter ν is determined from the required power level. Finally, the specification of the lab frame beam energy γ' and the cyclotron frequency parameter X' is based on extensive numerical calculation of efficiency in the (γ', X') parameter space.

Sensitivity of the efficiency to small variations in the relativistic electron cyclotron frequency requires that the beam energy and the external magnetic field be controllable within an accuracy of $\leqslant 1\%$.

The authors would like to thank Dr. T. Godlove, Dr. R. Parker, Dr. M. Reed, and Dr. P. Sprangle for many helpful discussions.

Appendix A

CONVERSION FORMULAE

Theoretical calculations in the present work are carried out in beam frame and parameters are normalized according to Eqs. (3)-(6). In this appendix, we tabulate the formulae needed to convert beam frame normalized quantities to lab frame phyical quantities. Column 2 of Table II converts the beam frame normalized quantities in column 1 to lab frame normalized quantities. The information needed for the conversion is the axial velocity v_z (in lab frame) which defines the quantity γ_z in column 2,

$$\gamma_z \equiv [1 - v_z^2/c^2]^{-1/2}.$$

Formulae presented in column 2 are based on the Lorentz transform. Derivations are obvious except for the following items.

$$(i) \quad \eta = \eta' \gamma_z (\gamma' - 1)/(\gamma_z \gamma' - 1) \tag{A.1}$$

To derive Eq. (A.1), we note that the time averaged EM field energy per unit length is (for TE_{on} mode)

$$< W_f > = \frac{K B_z^2 \omega^2}{8\pi \omega_c^2}$$

where K is a geometrical factor, B_z is the axial wave magnetic field amplitude, and ω_c is the waveguide cutoff frequency.

The injected beam energy per unit length is

$$W_b = N(\gamma - 1)mc^2$$

where N is defined in the text.

The lab frame efficiency (η) can therefore be written

$$\eta = \frac{< W_f >}{W_b} = \frac{K B_z^2 mc^2 \omega^2}{8\pi\omega_c^2 N(\gamma - 1)} \tag{A.2}$$

In Eq. (A.2) K, B_z and ω_c are all frame independent quantities.

The beam frame efficiency (η') is also expressed by Eq. (A.2) with ω, N, and γ replaced by ω', N', and γ' respectively. Thus

$$\frac{\eta}{\eta'} = \frac{\omega^2 N'(\gamma' - 1)}{\omega'^2 N(\gamma - 1)} \tag{A.3}$$

Since $\omega = \gamma_z \omega'$, $\gamma = \gamma_z \gamma'$, and $N = \gamma_z N'$, substitution of these relations into Eq. (A.3) yields Eq. (A.1).

(*ii*) $\omega_r = \gamma_z \omega_r'$ and $\omega_i = \omega_i'/\gamma_z$

In the beam frame, $k_z' = 0$. Hence all quantities vary as $\exp(-i\omega' t')$. To transform this expression into the lab frame, we use the relation $t' = \gamma_z (t - v_z z/c^2)$ and obtain

$$\exp(-i\omega' t') = \exp[-i(\omega_r' + i\omega_i')\gamma_z (t - v_z z/c^2)]$$

$$= \exp\left[-i\gamma_z \omega_r' t + i\frac{\gamma_z \omega_r' v_z}{c^2} z + \gamma_z \omega_i' t - \frac{\gamma_z \omega_i' v_z}{c^2} z\right].$$

Thus, the $\exp(-i\omega' t')$ dependence, viewed from the lab frame, has the following wave frequency (ω_r) and wave number (k_z),

$$\omega_r = \gamma_z \omega_r'$$

$$k_z = \gamma_z \omega_r' v_z/c^2$$

and, if one follows a beam segment (i.e. let $z = v_z t$), one observes a growth rate given by

$$\omega_i = \gamma_z \omega_i' (1 - v_z^2/c^2) = \omega_i'/\gamma_z.$$

Column 3 converts the lab frame normalized quantities in column 2 to lab frame physical quantities. The conversion formulae are based on Eqs. (3)-(5) in the main text. The informa-

tion needed at this step is the waveguide radius r_w, which can be determined from the desired wave frequency through

$$r_w = \bar{\omega}_r c/2\pi f, \tag{A.4}$$

where $\bar{\omega}_r$ is the calculated wave frequency (normalized) and f is the desired wave frequency in Hz.

From the lab frame physical quantities in column 3, we can derive the beam current (I_b), beam power (P_b), the maximum output wave power (P_w), and the power gain G:

$$I_b = \nu mc^2 v_z/e = 1.707 \times 10^4 \nu v_z/c \quad \text{Amp}, \tag{A.5}$$

$$P_b = I_b(\gamma - 1)mc^2 = 8.535 \times 10^6 \nu(\gamma - 1)v_z/c \quad \text{kW}, \tag{A.6}$$

$$P_w = \eta P_b, \tag{A.7}$$

$$G = 8.7\omega_i/v_z \quad \text{dB/unit length}. \tag{A.8}$$

REFERENCES

1. R. Q. Twiss, "Radiation Transfer and the Possibility of Negative Absorption in Radio Astronomy", Australian J. Phys. **11**, 564-579 (1958).
2. J. Schneider, "Stimulated Emission of Radiation by Relativistic Electrons in Magnetic Field", Phys. Rev. Lett. **2**, 504-505 (1959).
3. A. V. Gapanov, "Interaction Between Electron Fluxes and Electromagnetic Waves in Waveguides", Izv. VUZ., Radiofizika **2**, 450-462 (1959) and "Addendum", Izv. VUZ., Radiofizika **2**, 836 (1959).
4. J. L. Hirshfield and J. M. Wachtel, "Electron Cyclotron Maser", Phys. Rev. Lett. **12**, 533-536 (1964).
5. V. A. Flyagin, A. V. Gapanov, M. I. Petelin and V. R. Yulpatov, "The Gyrotron", IEEE Trans. **MTT-25**, 514-521 (1977).

6. J. L. Hirshfield and V. L. Granatstein, "The Electron Cyclotron Maser — An Historical Survey", IEEE Trans. **MTT-25**, 522-527 (1977).

7. V. L. Granatstein, M. Herndon, P. Sprangle, Y. Carmel and J. A. Nation, "Gigawatt Microwave Emission from an Intense Relativistic Electron Beam," Plasma Physics **17**, 23-28 (1975).

8. V. L. Granatstein, M. Herndon, R.K. Parker and S.P. Schlesinger, "Strong Submillimeter Radiation from Intense Relativistic Electron Beams", IEEE Trans. **MTT-22**, 1000-1005 (1974).

9. M. Friedman and M. Herndon, "Emission of Coherent Microwave Radiation from a Relativistic Electron Beam Propagating in a Spatially Modulated Field", Phys. Fluids **16**, 1982-1995 (1973).

10. N. I. Zaytsev, T.B. Pankratova, M. I. Petelin and V. A. Flyagin, "Millimeter and Submillimeter Waveband Gyrotrons", Radio Engineering and Electronic Physics **19**, 103-107 (May 1974).

11. D. V. Kisel', G. S. Korablev, V. G. Navel'yev, M. I. Petelin and Sh. E. Tsimring, "An experimental Study of a Gyrotron, Operating at the Second Harmonic of the Cyclotron Frequency, with Optimized Distribution of the High Frequency Field", Radio Engineering and Electronic Physics **19**, 95-100 (April 1974).

12. J. M. Wachtel and J. L. Hirshfield, "Interfernce Beats in Pulse-Stimulated Cyclotron Radiation," Phys. Rev. Lett. **17**, 348-351 (1966).

13. H. R. Jory, "Millimeter Wave Gyrotron Development - Phase I," Varian Associates, Inc., Report No. RADC-TR-77-210 (June 1977, unpublished).

14. V. L. Granatstein, P. Sprangle, M. Herndon, R. K. Parker, and S. P. Schlesinger, "Microwave Amplifiation with an Intense Relativistic Electron Beam," J. Appl. Phys. **46**, 3800-3805 (1975).

15. E. Ott and W. M. Manheimer, "Theory of Microwave Emission by Velocity-Space Instabil-

ities of an Intense Relativistic Electron Beam", IEEE Trans. **PS-3**, 1-5 (1975).

16. P. Sprangle and W. M. Manheimer, "Coherent Nonlinear Theory of a Cyclotron Instability," Phys. Fluids **18**, 224-230 (1975).

17. P. Sprangle and A. T. Drobot, "The Linear and Self Consistent Nonlinear Theory of the Electron Cyclotron Maser Instability", IEEE Trans. **MTT-25**, 528-544 (1977).

Table I — Efficiency optimized operating parameters for the NRL gyrotron travelling wave amplifier, $\alpha = 1.5$, $f = 35$ GHz ($\lambda = 8.57$ mm).

ν (density parameter)	2.076×10^{-3}
V (electron energy)	70.82 keV
I_b (beam current)	9.48 Amp
η (effieciency)	51.0 %
P_b (beam power)	671.5 kW
P_W (wave power)	342.5 kW
B_o	12.87 kG
k_z	1.96 cm^{-1}
r_w	5.37 mm
r_o	2.52 mm
r_L	0.61 mm
r_1	1.91 mm
r_2	3.13 mm
$v_\perp/c$	0.401
v_z/c	0.268
G (power gain)	2.0 dB/cm

Table II — Formulae for transformation from beam frame into lab frame and for converting normalized quantities into physical quantities

Beam Frame Normalized Quantities	Lab Frame Normalized Quantities	Lab Frame Physical Quantities
ν'	$\nu = \gamma_z \nu'$	ν (dimensionless)
γ'	$\gamma = \gamma_z \gamma'$	γ (dimensionless)
η'	$\eta = \eta' \gamma_z (\gamma' - 1)/(\gamma_z \gamma' - 1)$	η (dimensionless)
$\bar{\omega}_r'$	$\bar{\omega}_r = \gamma_z \bar{\omega}_r'$	$\omega_r = \bar{\omega}_r c/r_w$
$\bar{\omega}_i'$	$\bar{\omega}_i = \bar{\omega}_i'/\gamma_z$	$\omega_i = \bar{\omega}_i c/r_w$
$\bar{k}_z'$	$\bar{k}_z = \gamma_z \bar{v}_z \bar{\omega}_r'$	$k_z = \bar{k}_z/r_w$
$\bar{\Omega}_e'$	$\bar{\Omega}_e = \bar{\Omega}_e'$	$\Omega_e = \bar{\Omega}_e c/r_w$
$\bar{r}_L'$	$\bar{r}_L = \bar{r}_L'$	$r_L = \bar{r}_L r_w$
$\bar{r}_1'$	$\bar{r}_1 = \bar{r}_1'$	$r_1 = \bar{r}_1 r_w$
$\bar{r}_2'$	$\bar{r}_2 = \bar{r}_2'$	$r_2 = \bar{r}_2 r_w$

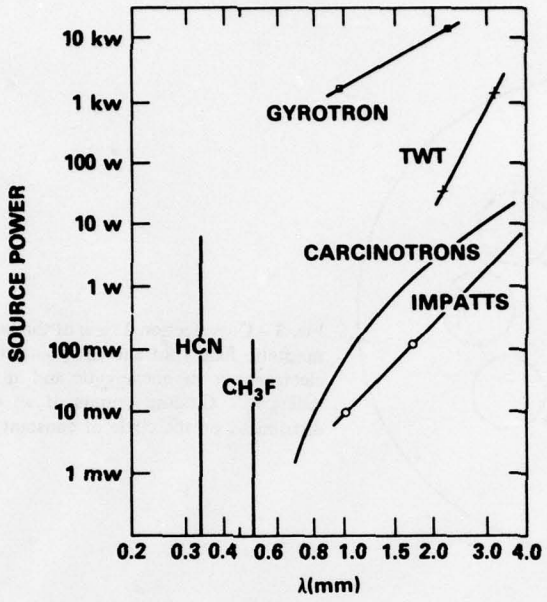

Fig. 1 – State-of-art CW power sources.

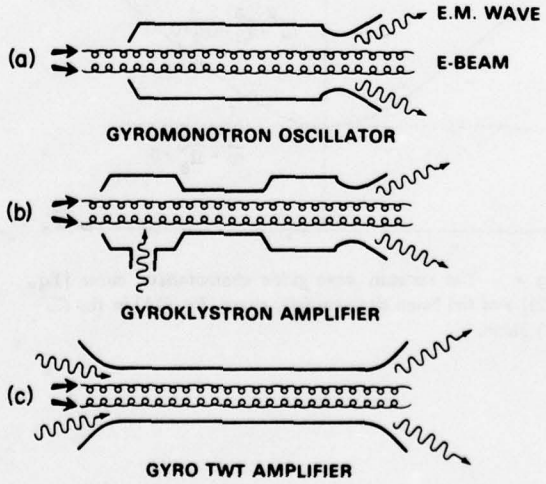

Fig. 2 – Type of gyrotrons.

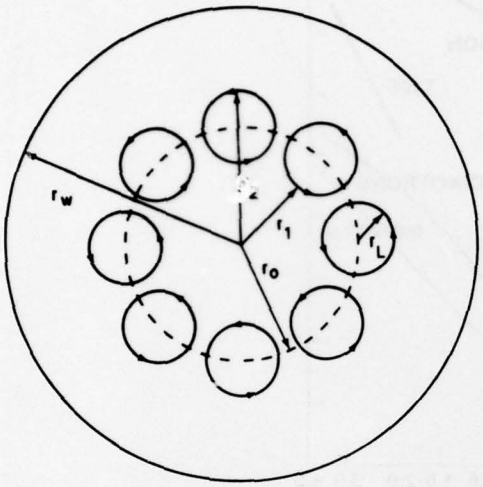

Fig. 3 – Cross-sectional view of the beam model. The applied magnetic field (not shown) points toward the reader. The electrons are monoenergetic and all have the same Larmor radius r_L. Guiding centers of all electrons are uniformly distributed on the circle of constant radius r_o.

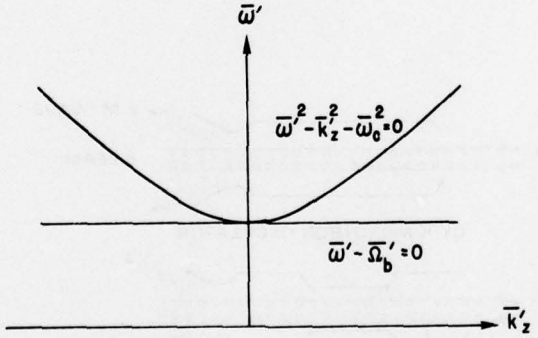

Fig. 4 – The vacuum wave guide characteristic curve [Eq. (10)] and the beam characteristic curve [Eq. (11) in the ($\bar{\omega}'$, $\bar{k}_z$) plane.

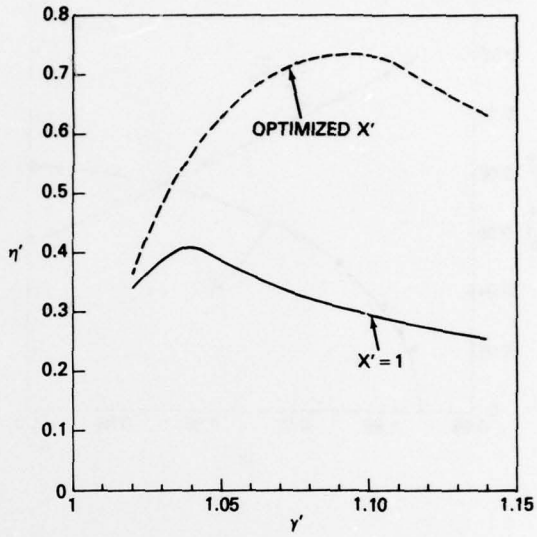

Fig. 5 – η' versus γ' for grazing intersection case ($X' = 1$, solid curve) and for optimized near grazing intersection case ($X' < 1$, dashed curve). A point on the dashed curve, $\eta'(\gamma', X')$, is obtained by varying X' but keeping γ' fixed until $\eta'(\gamma', X')$ reaches a maximum, illustrated in Fig. 6. The peak of the dashed curve is therefore the peak of η' in the (γ', X') parameter space. The parameters used for this figure are $\bar{r}_0 = 0.48$, $\nu' = 0.002$, and $\bar{k}'_z = 0$.

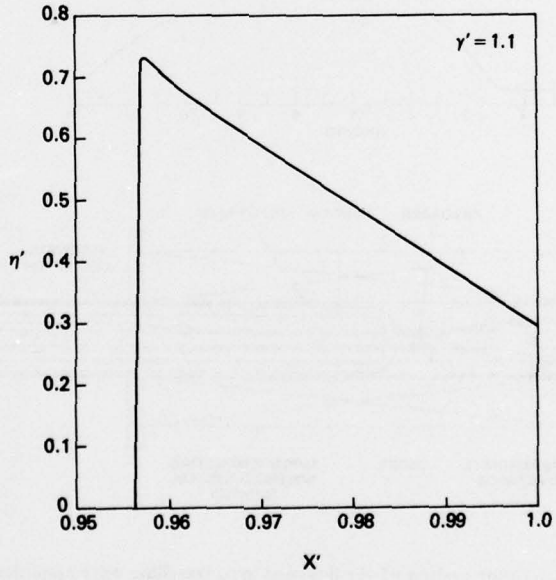

Fig. 6 – Efficiency η versus X' for $\gamma' = 1.1$, $\bar{r}_0 = 0.48$, $\nu' = 0.002$, and $\bar{k}'_z = 0$.

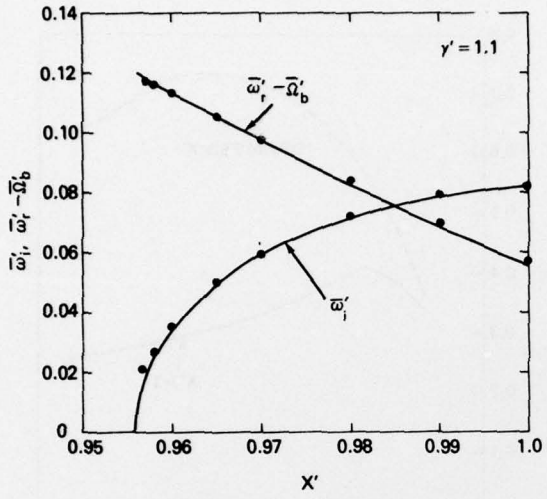

Fig. 7 – Growth rate $\bar{\omega}_i'$ and frequency shift $\bar{\omega}_r' - \bar{\Omega}_b'$ versus X' for $\gamma' = 1.1$, $\bar{r}_0 = 0.48$, $\nu' = 0.002$, and $\bar{k}_z' = 0$. $\bar{\omega}_r'$, and $\bar{\Omega}_b'$ are, respectively, the wave frequency and beam electron cyclotron frequency.

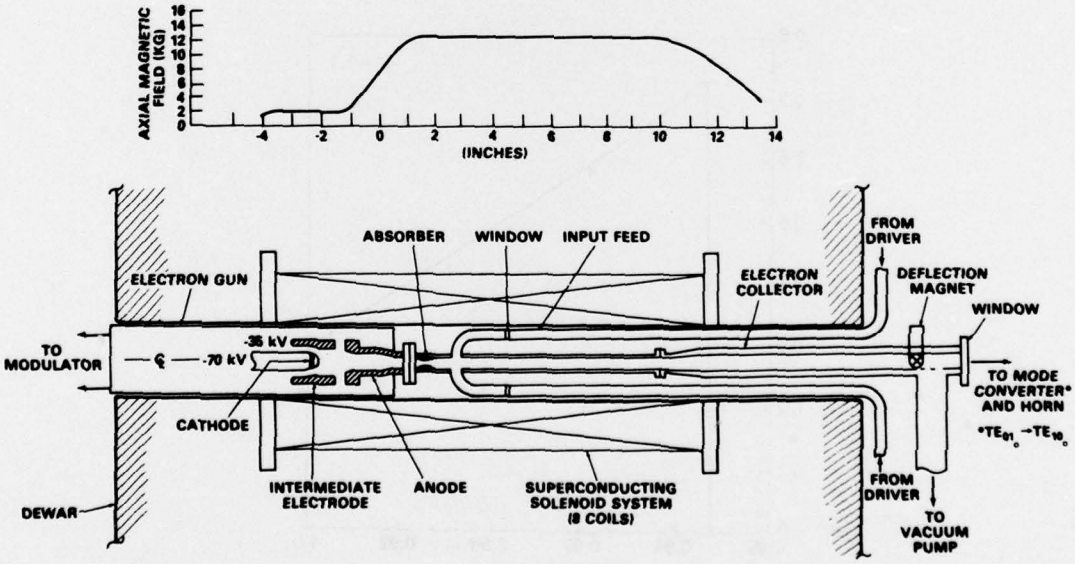

Fig. 8 – Configuration of the designed gyro travelling wave amplifier.